Received: 23 April 2021 | Revised: 7 December 2021 | Accepted: 9 December 2021

DOI: 10.1002/jbm.b.35005

RESEARCH ARTICLE

Nanosized calcium deficient hydroxyapatites for tooth enamel protection

Vita Zalite[1] | Janis Lungevics[2] | Jana Vecstaudza[1] | Liga Stipniece[1] | Janis Locs[1,3]

[1]Rudolfs Cimdins Riga Biomaterials Innovations and Development Centre of RTU, Institute of General Chemical Engineering, Faculty of Materials Science and Applied Chemistry, Riga Technical University, Riga, Latvia

[2]Department of Mechanical Engineering and Mechatronics, Faculty of Mechanical Engineering, Transport and Aeronautics, Riga Technical University, Riga, Latvia

[3]Baltic Biomaterials Centre of Excellence, Headquarters at Riga Technical University, Riga, Latvia

Correspondence
Vita Zalite, Rudolfs Cimdins Riga Biomaterials Innovations and Development Centre of RTU, Institute of General Chemical Engineering, Faculty of Materials Science and Applied Chemistry, Riga Technical University, Riga, Latvia.
Email: vita.zalite@rtu.lv

Funding information
European Regional Development Fund, Grant/Award Number: 1.1.1.2/VIAA/3/19/459; European Union's Horizon 2020, Grant/Award Number: 857287

Abstract

Calcium phosphates (CaP) are extensively studied as additives to dental care products for tooth enamel protection against caries. However, it is not clear yet whether substituted CaP could provide better enamel protection. In this study we produced, characterized and tested in vitro substituted and co-substituted calcium deficient hydroxyapatite (CDHAp) with Sr^{2+} and F^{-} ions. X-ray powder diffractometry, Fourier transformation infrared spectroscopy, scanning electron microscopy, energy-dispersive X-ray analysis, Brunauer–Emmett–Teller were used to characterize synthesized powders and also cytotoxicity was evaluated. pH = f(t) test was performed to estimate, weather synthesized CDHAp suspensions are able to increase pH of experimental media after acid addition. Synthesis products were incorporated into paste to perform in vitro remineralization on the bovine enamel. In addition to mentioned instrumental methods, profilometry was used for evaluation of remineralised enamel samples. The obtained results confirmed formation of CDHAp substituted with 1.5–1.6 wt% of fluoride and 7.4–7.8 wt% of strontium. pH = f(t) experiment pointed out that pH increased by approximately 0.3 within 10 min after acid addition for all CDHAp suspensions. A new layer of the corresponding CDHAp was formed on the enamel. Its thickness increased by 0.8 ± 0.1 μm per day and reached up to 5.8 μm after 7 days. Additionally, octa calcium phosphates were detected on the surface of control samples. In conclusion, we can assume that CDHAp substituted with Sr^{2+} and/or F^{-} could be used as an effective additive to dental care products promoting formation of protecting layer on the enamel, but there was no significant difference among sample groups.

KEYWORDS
calcium phosphate, enamel protection, nanoparticles, tooth enamel

1 | INTRODUCTION

Calcium phosphates (CaPs), mainly hydroxyapatite (HAp), due to their chemical and structural similarity with bone and teeth mineral components are widely used for replacement, regeneration, and augmentation of calcified tissue.[1,2] As resolved previously,[3–5] biological HAp is not stoichiometric and may contain various amounts of substitutions (i.e., F^{-}, HPO_4^{2-}, CO_3^{2-}, Na^{+}, Mg^{2+}, Sr^{2+}). Many synthesis

methods have been developed to produce substituted and non-stoichiometric HAp with different particle morphology.[6–15] Such materials can be used for preventive dentistry as an active additive to dental care products.

In the last two decades CaPs nanomaterials have been studied as remineralizing agents for tooth enamel protection from early caries.[16–18] In the scientific literature two processes are proposed to explain the CaPs protective effect on tooth enamel. It has been suggested that CaPs can boost the remineralization of lost minerals due to their ability to release Ca^{2+} and PO_4^{3-} ions, thus supplying mouth cavity with extra Ca^{2+} and PO_4^{3-} ions.[19,20] The other process is associated with CaPs particles that easily block dentine tubules or settle on the enamel surface defects.[21,22]

Calcium deficient hydroxyapatite (CDHAp) is potentially a good alternative to stoichiometric HAp to grant additional functionality. It can be easily substituted with various ions. Accordingly, we chose fluoride ions (F^-) for substitution of hydroxyl ions (OH^-) due to verified anti-caries performance in clinical studies for many decades,[23] and strontium ions (Sr^{2+}) for substitution of calcium ions (Ca^{2+}), as strontium salts are being introduced into dentifrice for desensitizing purposes.[24] Moreover, some study confirmed uptake of F^- and Sr^{2+} by plaque, thereby affecting metabolism of bacteria and inhibiting formation of bacterial acids[25,26] that are critical for inhibition of caries. Fluoride ions replace hydroxyl ions into CDHAp structure, thus improving mechanical properties and decreasing solubility, leading to resistance against acids secreted by bacteria in plaque.[27,28] J. Fearthersone cites three reasons why fluoride is effective against caries: (i) inhibits bacterial metabolism, (ii) inhibits demineralization at the crystal surface during an acid challenge, (iii) enhancing remineralization and thereby forming a low-solubility layer similar to the acid resistant mineral fluorapatite, on the remineralized crystals. Studies in caries research have shown that only if fluoride is introduced into a new crystal surface during remineralization, it beneficially altered enamel solubility.[29] Strontium mostly is known for its ability to prevent bone resorption as well as confront osteoporosis,[30] but in dentistry in the very beginning it has been used for teeth desensitizing effect as mentioned previously. Recently, Krishnan et al. observed, that incorporation of Sr^{2+} up to 25 mol% into HAp structure increases cell viability compared to pure HAp phase, that is important factor for well-being of tissues in the mouth cavity.[31] Also, scientists from Italy noticed better mineralization of hard tissues for Sr^{2+} containing samples.[32]

Simultaneous addition of Sr^{2+} and F^- to bioactive glasses has been studied.[33–36] The findings showed, that incorporation of these two ions into bioactive glass had beneficial and synergistic effects on HAp crystallization and pH increase was observed in the research media, thus reducing loss of minerals and promoting remineralization of demineralized enamel and dentine. Moreover, beneficial antibacterial effect was observed for glass ionomers with Sr^{2+} and F^-.[30]

Taking into account the studies described above, we have concluded, that there is luck of information about simultaneous incorporation of strontium and fluoride ions into CDHAp structure. CDHAp chemical and crystal structure is more similar to natural tooth enamel and dentine comparing to bioactive glasses. We were curious, is there any difference of remineralization potential among pure CDHAp and substituted CDHAp? Therefore, in current study we synthesized needle-like Sr and/or F substituted CDHAp and evaluated enamel recovery ability with the same materials. Also the possibility to protect enamel from caries and erosion caused by acidic environment was evaluated. In vitro tests, simulating application of dental care products containing substituted CDHAp nanoparticles on bovine teeth enamel were performed. Special attention was paid for in vitro remineralization equipment and experimental design. Our findings are complementary to the field of remineralizing agents used in dentifrice, toothpastes, mouthwashes, and so forth.

2 | MATERIALS AND METHODS

Our research had two parts—synthesis and characterization of CaP and remineralization studies (see Figure 1). Remineralization study includes preparation of CaP pastes and in vitro studies, where bovine enamel samples were treated.

2.1 | Preparation and characterization

2.1.1 | Wet chemical precipitation

All CDHAp were synthesized trough wet precipitation method according to these parameters: Ca/P or Ca + Sr/P molar ratio between 1.50 and 1.67, theoretical Sr substitution level 10 wt% in respect to total weight of the product and theoretical F substitution level 3 wt% in respect to total weight of the product.

To obtain CDHAp, CaO was used as calcium source from which $Ca(OH)_2$ suspension was obtained. Subsequently, neutralization reaction between 0.3 M $Ca(OH)_2$ and 2 M H_3PO_4 at 45°C was realized. H_3PO_4 addition was done by incremental mode till end pH 7.2, then CaP suspension was stirred for 1 h and vacuum filtered.

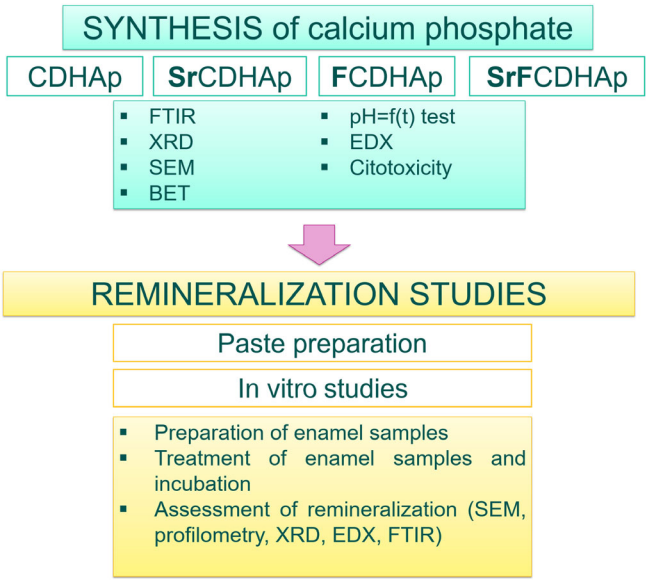

FIGURE 1 A schematic illustration of experimental methods

Sr substituted CDHAp (SrCDHAp) production was done as described above and SrO was used as Sr source.

The synthesis of F substituted CDHAp (FCDHAp) had two stages: (i) production of CDHAp, (ii) pH-cycling of obtained CDHAp suspension to incorporate fluorine into the structure. Stage (ii) included addition of 0.09 M NH_4F solution with following pH-cycling of obtained suspension. The pH of the suspension was lowered to 4 by addition of 2 M H_3PO_4 and subsequentialy raised to 7 by incremental addition of 1 M NaOH solution. Described pH cycling was repeated three times. The end stage of the FCDHAp synthesis was the washing of obtained precipitates with deionized water during vacuum filtration process.

To obtain SrFCDHAp precipitates we combined SrCDHAp and FCDHAp production techniques sequentially.

For determination of phase composition and evaluation of characteristic absorption bands part of the filtered precipitates was dried and calcined at 1100°C (1 h). Remaining wet precipitates were stored in a fridge at 4°C into the closed containers till further use for experiments.

2.1.2 | Physico-chemical characterization

The phase composition and characteristic functional groups of the powders were investigated using X-ray powder diffractometry (XRD, PANalytical X'Pert Pro, Cu Kα1, 40 kV, 30 mA) and Fourier transformation infrared spectroscopy (FTIR, Varian Scimitar 800, KBr pellet method at 4 cm^{-1} resolution co-adding 30 scans over a range of wavenumbers from 400 to 4000 cm^{-1}). The morphology of synthesized products was observed with field emission scanning electron microscopy (FE-SEM, Tescan Mira/LMU), and high-resolution transmission electron microscopy (HR-TEM, Tecnai G20) with a field emission gun operating at 200 kV. Fluorine content was determined by elemental analysis using energy-dispersive x-ray analysis (EDX, Oxford Instruments X-Max^N detector size 150 mm^2). Strontium content was analyzed by AAS (Varian SpetrAA880). Crystallite size (d) were calculated from XRD pattern using Scherrer equation[37] at $2\theta = 25.9°$, corresponding to the 002 hkL crystal plane. Brunauer–Emmett–Teller (BET) method was used to determine specific surface area (SSA) of the precipitated powders by N_2 absorption (Quadrasorb SI-KR/MP, Quantachrome Instruments). Equivalent particle diameter (d_{BET}) was calculated using following equation:

$$d_{BET} = \frac{6}{q \times Sw}, \quad (1)$$

where q is the true density of CDHAp powder (g/cm^3) and Sw is the SSA. Density measurements of synthesized CDHAp powders were done with helium pycnometer Micro UltraPyc 1200e (Quantachrome Instruments, Boynton Beach, Florida, USA).

The evaluation of bovine enamel samples was carried out with following instrumental methods. XRD patterns were recorded using Ni filtered monochromatized Cu Kα1 radiation ($\lambda = 0.1540$ nm) generated at 40 kV and 30 mA and in the 2θ range from 5° to 70°. FTIR spectra were recorded in the attenuated total reflectance (ATR, GladiATR™, Pike technologies, USA) mode and obtained at 4 cm^{-1} resolution co-adding 50 scans over a range of wavenumbers from 400 to 4000 cm^{-1}. Before every measurement, a background spectrum was taken and deducted from the sample spectrum. XRD and FTIR were taken for etched and treated enamel samples. The surfaces of demineralized and remineralized samples were observed with SEM at an accelerating voltage 15 kV and images were taken under 30,000× and 100,000× original magnification. The thickness of newly formed CaP layer on the enamel slabs were analyzed by contact type 3D profilometer (Taylor Hobson Form Talysurf Intra 50). The scanning speed was set to 1 mm/s and standard stylus 112–2009 with probe tip radius 2 μm was used.

2.1.3 | Ability to increase pH of acidic media

We tested ability of the nanoparticles to increase pH of acidic media, thus mimicking acidic environment in the oral cavity after a meal. The experimental set-up is shown in Figure 2. For this experiment, 5 mg of the nanoparticles were dispersed into 40 ml H_2O and homogenized with sonotrode Hielscher for 10 s (amplitude 59%, 82 W). Titration station Mettler Toledo with software LabX and pH sensor was adapted to perform the experiment. Following process steps were done:

1. Heating of the nanoparticles suspension up to 36°C (in a water bath);
2. Addition of 10 μl of 0.05 M citric acid every 10 min (maximum 90 μl). The selected time period was chosen according to the results from preliminary experiments, in which a plateau occurred on the pH change curve after 10 min.
3. After the addition of the last 10 μl of citric acid, pH changes of the system were observed for 30 min.

2.1.4 | Cytotoxicity

Samples for cytotoxicity were prepared from wet precipitates. For the preparation of the test samples, the moisture content of each paste

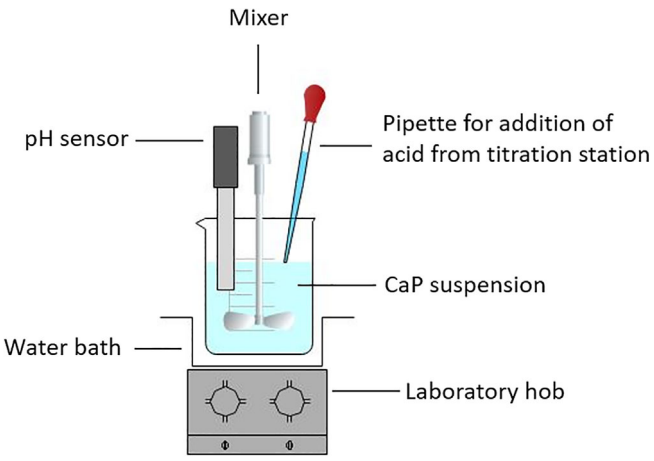

FIGURE 2 A schematic illustration of experimental equipment to test the ability of the nanoparticles to increase pH of acidic media

has been taken into account to obtain suspensions with concentrations 300 and 500 μg/ml.

For the assessment of cytotoxicity of the nanoparticles, cell line HGF-1 (ATCC® CRL-2014™) was used. Dulbecos modified eagle medium (DMEM, Millipore) and 10% fetal bovine serum (FBS, Millipore) was used as a cultivation media in 24 well plate. Approximately 180,000 cells were seeded in each well. Cells were cultivated for 24 h prior to expose of test material. After 48 h incubation at 37°C and 5% CO_2 in the atmosphere, test material was removed and cells detached from reaction plate surface. Hemocytometer was used for cell counting. ANOVA test was applied for data statistical analysis, where $p = .05$.

2.2 | Preparation of pastes

To evaluate ability of the nanoparticles to protect enamel hard tissue, a simple composition of pastes was created. Water, glycerol, 2-hydroxycellulose (HOECel) and relevant synthesis product were used (See Table 1). To obtain homogeneous mas, IKA T18 basic ULTRA-TURRAX homogenizer and sonotrode UP200t Hielscher (82 W, amplitude 49%, 2 min) was used to frustrate larger agglomerates and to reduce the number of air bubbles into the paste. The amounts of used components are summarized in Table 1.

The viscosity of prepared pastes was measured with rotational viscometer RheolabQC (Anton Paar) at 5 rpm for 10 min and it was comparable with commercial toothpaste BioRepair®. According to ISO 11609:2010 the pH of all pastes was under 10.5.

2.3 | Mineralization study in vitro

2.3.1 | Preparation of bovine enamel blocks

Enamel blocks were prepared from bovine teeth (obtained as by-products from slaughterhouse). Bovine teeth were cleaned from soft tissue debris, then each tooth was sectioned horizontally below the cementoenamel junction using a water-cooled diamond saw (IsoMet Low Speed Saw). Soft tissue debris from pulp cavity were removed. All teeth were carefully rinsed under deionized water and stored in to 0.01% thymol solution at 4°C prior further use.

To obtain enamel blocks with surface dimensions 3×4 mm^2, tooth crown (lingual surface) was attached to the PE plate and labial surface of the crown was cut horizontally and vertically (Figure 3).

The surface of enamel blocks was prepared according to ISO 11609:2010. As the surface roughness of samples should not exceed 0.3 μm, bovine enamel blocks were grinded with sandpapers (600, 800, 1000, 1500 grit) for 5 min. Grinding procedure also removed plaque and dental calculus from the surface. Afterwards the samples were washed into the ultrasound bath for 5 min to remove dusts from the enamel surface. The roughness of surface was measured by 3D profilometry to be in conformity with ISO standard.

Before in vitro studies, enamel samples were subjected to demineralization to obtain exposed enamel tissue structure. The surfaces of specimens were immersed in the 34% H_3PO_4 for 15 s, then rinsed with deionized water.[38]

Prepared specimens were embedded into special sample holder (see paragraph b.), where a half of each enamel block surface was covered with nail varnish to serve as an untreated control.

2.3.2 | Equipment for in vitro study

Custom made sample holders were prepared to ensure relatively equal experimental conditions (Figure 4). The sample holder was designed with closed cavity inside to have the ability to float. Such position of sample holder ensured that embedded enamel blocks were faced downwards, thus deposition of minerals from artificial saliva due to gravity was excluded during in vitro study. Moreover, during and after the experiment, it was not necessary to take out enamel specimens from the sample holder for surface treatment with the pastes and for physico-chemical analysis. To perform enamel surface brushing, we adapted, BUEHLER MINIMET 1000″ grinding machine by designing special frame for sample holder to fix it during treatment with the pastes (Figure 5).

Custom made sample holder was used also for XRD analysis (Figure 6), thus enamel block was positioned in the center of the holder. It should be noted that central sample was not coated with partly masking nail varnish.

2.3.3 | Treatment of enamel blocks with the pastes

The surface treatment of enamel samples was performed according to scheme shown in Figure 7.

Enamel blocks were placed in the artificial saliva (0.33 g KH_2PO_4, 1.27 g KCl, 0.58 g NaCl, 0.17 g $CaCl_2$, 0.2 g $[NH_2]_2CO$, 1 L deionized

TABLE 1 The composition of paste

Nr.	Paste designation	CaP (wt%)	HOECel (wt%)	Glycerin (wt%)	Water (wt%)
1.	Rem_CDHAp	20	3	5	72
2.	Rem_FCDHAp	20	3	5	72
3.	Rem_SrCDHAp	20	3	5	72
4.	Rem_SrFCDHAp	20	3	5	72

Abbreviations: CaP, calcium phosphates; CDHAp, calcium deficient hydroxyapatite; FCDHAp, F substituted CDHAp.

FIGURE 3 Preparation of bovine enamel blocks

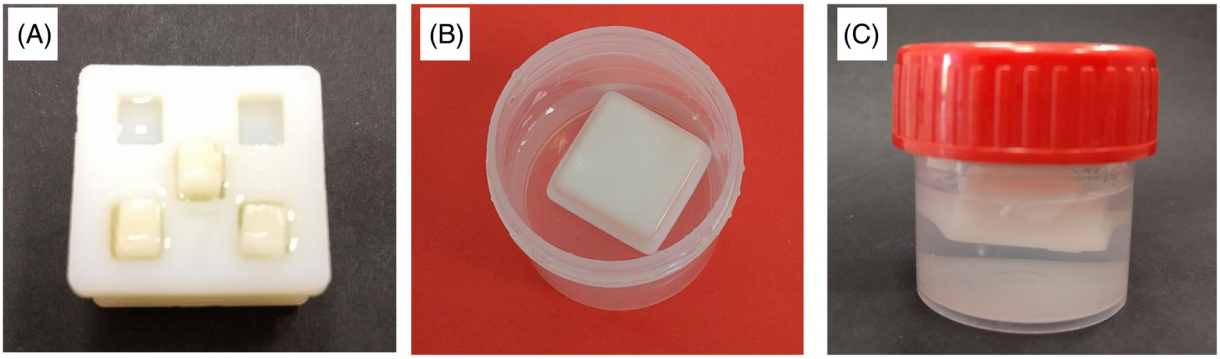

FIGURE 4 Sample holder for in vitro studies: (A) holder with tooth samples, (B and C) holder immersed in the artificial saliva

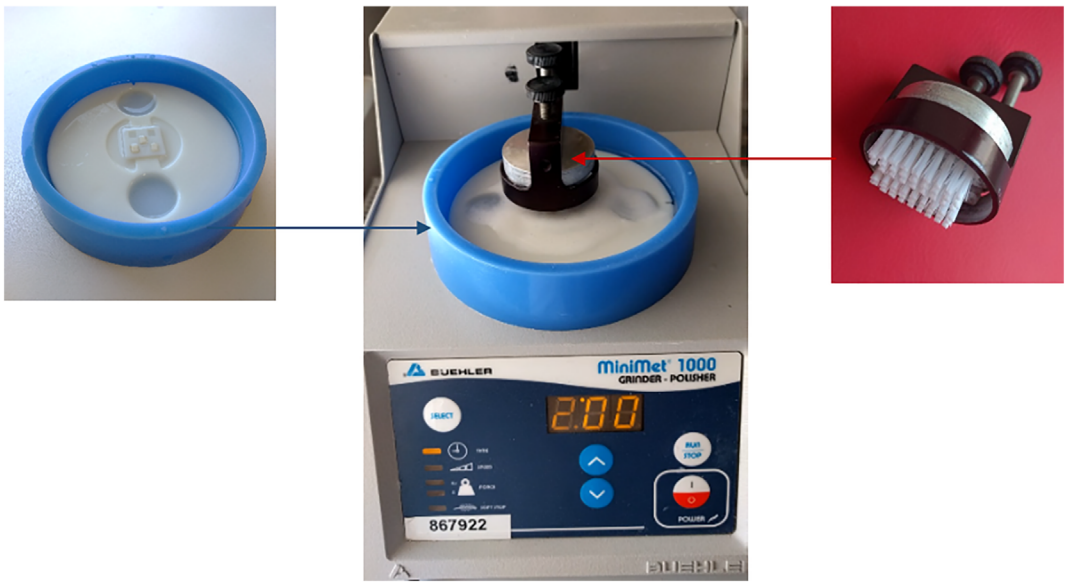

FIGURE 5 The equipment for treatment of enamel blocks with the pastes

H_2O) at 37°C. Incubator (Biosan Orbital Shaker – Incubator ES – 20) ensured dynamic condition (shelf rotation speed 100 rpm) between treatment episodes with pastes. To simulate everyday tooth brushing, following steps were performed (repeated two times a day for 7 days):

1. Removal of the sample from artificial saliva;
2. Sample rinsing with deionized water;
3. Sample demineralization with 50 mM citric acid for 3 min;
4. Sample rinsing with deionized water;

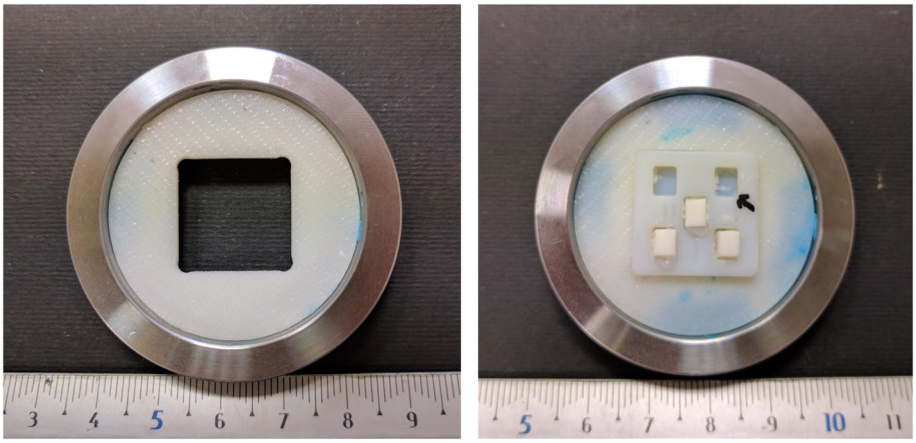

FIGURE 6 Custom made sample holder for XRD analysis. XRD, X-ray powder diffractometry

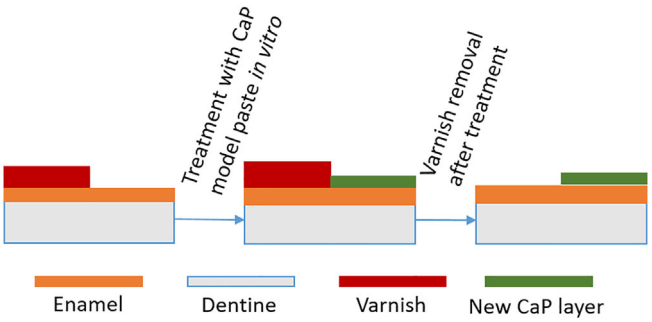

FIGURE 7 Schematic image of enamel sample treatment

5. Sample brushing with the pastes for 3 min with applied toothbrush force of 0.2 N per 1 cm^2;
6. Sample rinsing with deionized water;
7. Incubation of the sample in to the container with artificial saliva.

All experimental groups are summarized in Table 2.

After a set of in vitro experiments, nail varnish was removed and both sides of enamel surface investigated.

TABLE 2 Experimental groups

Sample group	Comment
Rem_Dynamic	• Treatment with Rem_CDHAp • Twice a day for 2 min • 5 days • Profilometry every day
Rem_Control	• Treatment without paste • Twice a day 2 min • 7 days
Rem_CDHAp	• Treatment with Rem_CDHAp • Twice a day 2 min • 7 days
Rem_SrCDHAp	• Treatment with Rem_SrCDHAp • Twice a day 2 min • 7 days
Rem_FCDHAp	• Treatment with Rem_FCDHAp • Twice a day 2 min • 7 days
Rem_SrFCDHAp	• Treatment with Rem_SrFCDHAp • Twice a day 2 min • 7 days

Abbreviations: CDHAp, calcium deficient hydroxyapatite; FCDHAp, F substituted CDHAp.

3 | RESULTS

Table 3 presents data obtained from XRD, BET, and EDX analyses. All synthesis products after thermal treatment are biphasic mixtures composed of HAp and β-tricalcium phosphate (β-TCP). According to EDX results, only 50% of added fluoride and 74%–78% of strontium were found into the FCDHAp, SrFCDHAp and SrCDHAp samples. The highest SSA values were measured for SrCDHAp following by CDHAp, SrFCDHAp, and FCDHAp. We observed that fluoride incorporation into CDHAp structure results in lower values of SSA compared to CDHAp and SrCDHAp powders. Calculated particle size of all synthesis products ranges from 22 to 29 nm and are close to calculated crystallite size (d_{002}).

3.1 | Physico-chemical characterization

FTIR showed characteristic absorbance bands of (PO_4) and (OH) groups for all synthesized powders. Additionally, the spectra showed absorbance bands characteristic to (HPO_4) and (CO_3) functional groups. The presence of (CO_3) absorbance bands is attributed to atmospheric CO_2 in the synthesis environment and its inclusion in the product structure. In turn, the presence of (HPO_4) confirms that the products are CDHAp.[39] In the FTIR spectra of the thermally treated powders the respective absorbance bands were not detected, while extra maximums at 3543–3547 cm^{-1} and 735 cm^{-1} were detected for FCDHAp, and SrFCDHAp spectra.

XRD patterns of the synthesized powders showed crystalline structure with low crystallinity, as evidenced by relatively broad and low-intensity XRD peaks. Diffraction peaks of the powders became

sharper and with higher intensity after thermal treatment at 1100°C, indicating increase of crystallinity. A slight shifting of maximums toward smaller 2θ angle were observed for Sr containing powders due to Sr incorporation into CDHAp structure.

SEM and TEM evaluation (Figure 8) shows needle-like morphology for all synthesized particles. In addition, TEM investigation reveals that observed particles actually were agglomerates consisting of smaller units and nanoparticles morphology was close to natural tooth crystals 50–70 nm in width and 20–25 nm in thickness.[40]

3.2 | Ability to increase pH of acidic media

Figure 9 represents the ability of nanoparticles to balance the pH of aqueous systems after acid addition. In all experiments, a steep decrease of pH after addition of 50 mM citric acid was observed. In case of enamel sample, pH decreased by 2.5 units; this means, the critical pH level was passed (pH ≤5.5[41]) and enamel started to dissolve irreversibly, but for synthesized nanoparticle suspensions, pH decreased only by 1.0–1.2 units. After 10 min we observed uplift of the curves, thus indicating a slight compensation effect of pH drop in the aqueous systems. Comparing all four suspensions, relatively higher pH values was maintained for SrCDHAp, but the lowest pH was for SrFCDHAp suspension.

3.3 | Cytotoxicity

The results of cytotoxicity studies showed that among various concentrations of the nanoparticles suspensions, a significant reduction of gingival fibroblast cell viability occurred in the case of SrCDHAp and FCDHAp samples. CDHAp and SrFCDHAp suspensions in various concentrations do not significantly affect the cell viability. Cytotoxic samples are marked with the "#" symbol in Figure 10.

3.4 | Remineralization in vitro

3.4.1 | Fourier transformation infrared spectroscopy

Figure 11 summarizes FTIR spectra from all enamel samples and spectrum of 2-hydroxyethyl cellulose, as it was used as component for the

TABLE 3 Characteristics of synthesized nanopraticles

	FCDHAp	SrCDHAp	SrFCDHAp	CDHAp
Ca/P ratio	1.64			1.65
Ca + Sr/P ratio		1.64	1.64	
HAp/β-TCP, wt %[a]	86/14	82/12	84/16	89/11
F, wt %	1.6 ± 0.1	–	1.5 ± 0.2	–
Sr, wt %	–	7.4 ± 0.4	7.8 ± 0.3	–
SSA, m^2/g	71.1 ± 0.2	94.5 ± 1.3	78.1 ± 0.4	82.3 ± 0.8
Particle size d_{BET}, nm	29.7 ± 0.1	22.6 ± 0.3	26.5 ± 0.1	25.3 ± 0.2
Crystallite size d_{002}, nm	30	27	27	27

Abbreviations: CDHAp, calcium deficient hydroxyapatite; FCDHAp, F substituted CDHAp; HAp, hydroxyapatite; SSA, specific surface area.
[a]After thermal treatment at 1100°C for 1 h.

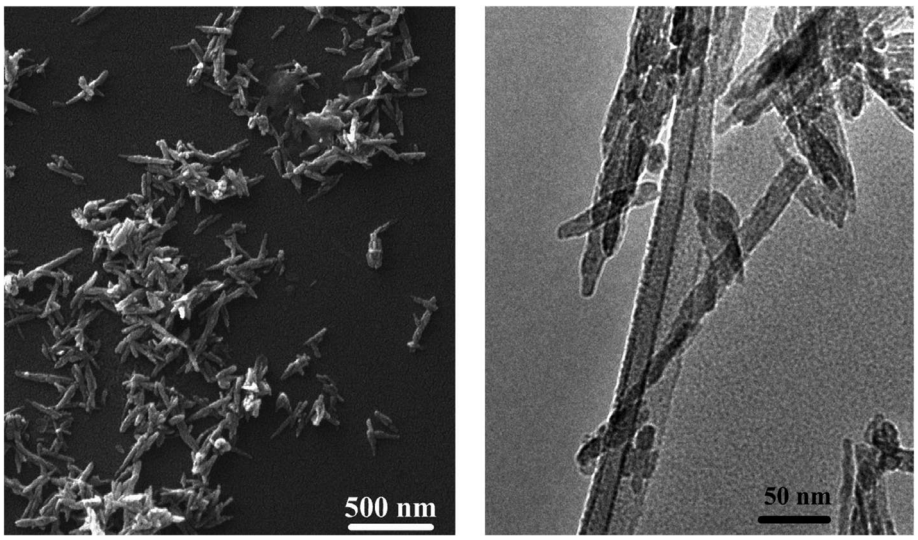

FIGURE 8 Morphology of the synthesized powders; left—SEM image, right—TEM image. SEM, scanning electron microscopy; TEM, transmission electron microscopy

pastes. The peaks and broad bands in the HOCel graph are attributed to (OH) (3000–3600 cm^{-1}), (C—H) (2900–2999 cm^{-1} and 1249–1454 cm^{-1}), (C—O) (1030 cm^{-1}), and adsorbed H_2O from atmosphere (1650 cm^{-1})[42–44] FTIR data of enamel samples showed major chemical groups of CaP. The absorbance bands of (PO_4) group were detected from 472 cm^{-1} to 599 cm^{-1} for etched enamel, control and all treated samples. The overlap of (PO_4) and (HPO_4) vibrations occurred from 720 cm^{-1} to 1160 cm^{-1}, while characteristic vibration of (OH) group was recorded in the range 630–636 cm^{-1} and at ≈3565 cm^{-1} (Figure 12B; indicated with arrow). The absorbance bands of (CO_3) at 1410–1450 cm^{-1} were detected for all enamel samples. Additionally, absorbance bands of amide groups were found from 1560 cm^{-1} to 1530 cm^{-1} for remineralized samples. Bending of (N—H) group and stretching of (C—N) group came from tooth enamel organic component.[45] A small peak at 912 cm^{-1} (Figure 12A) for Rem_control. According to previous studies,[37,46] this place on the graph is attributed to (P-OH) absorption mode originating from octacalcium phosphate (OCP).

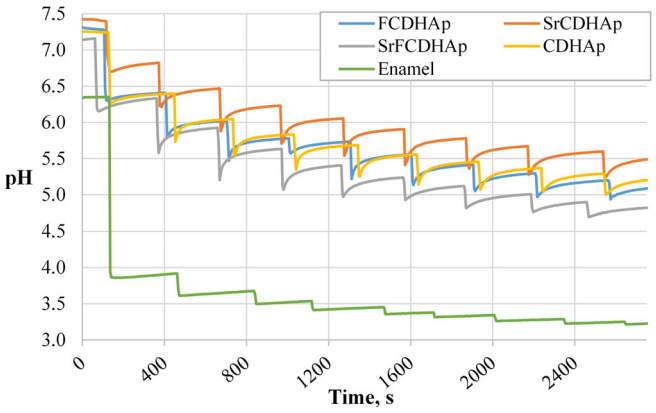

FIGURE 9 The function of pH in time for suspensions after incremental addition of acid

3.4.2 | X-ray powder diffractometry

XRD patterns were similar for all enamel samples. The only difference was observed for peak intensities. However, one diffraction peak at 32.86° 2θ (HAp, ICDD 01–072-1243) for treated enamel samples was

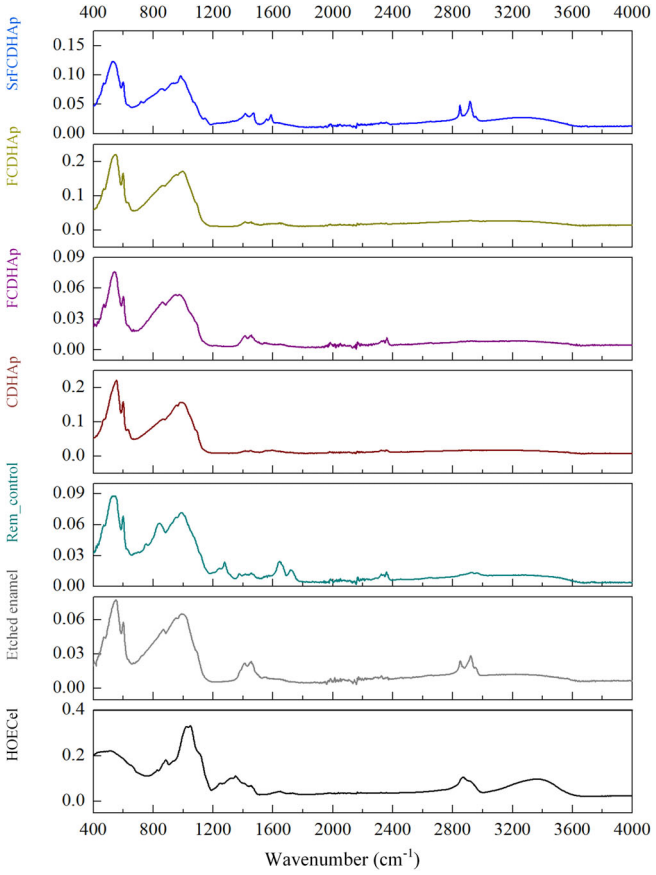

FIGURE 11 FTIR spectra of remineralized samples, control sample, etched enamel, and hydroxyethyl cellulose. FTIR, Fourier transformation infrared spectroscopy

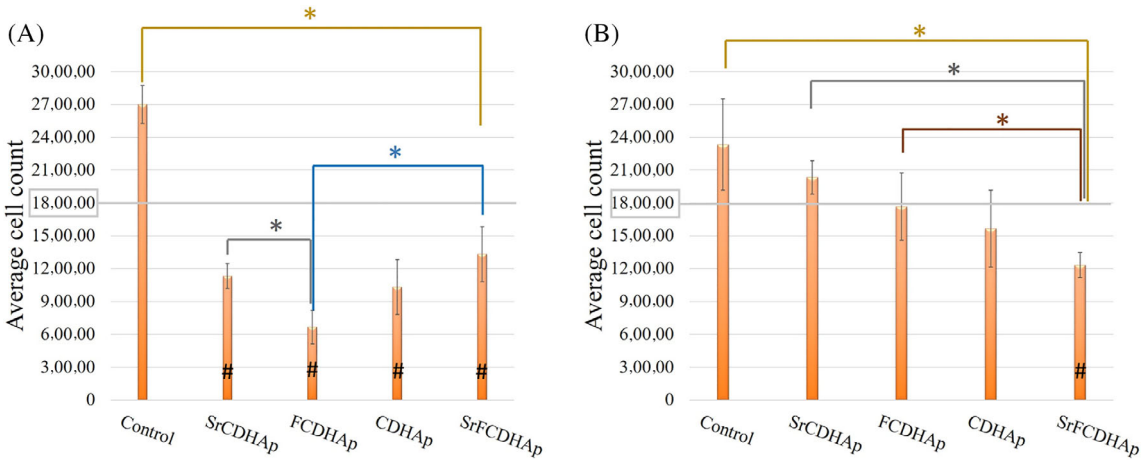

FIGURE 10 Results of cytotoxicity studies of the nanoparticles in different concentrations: (A) 500 μg/ml, (B) 300 μg/ml; *$p < .05$

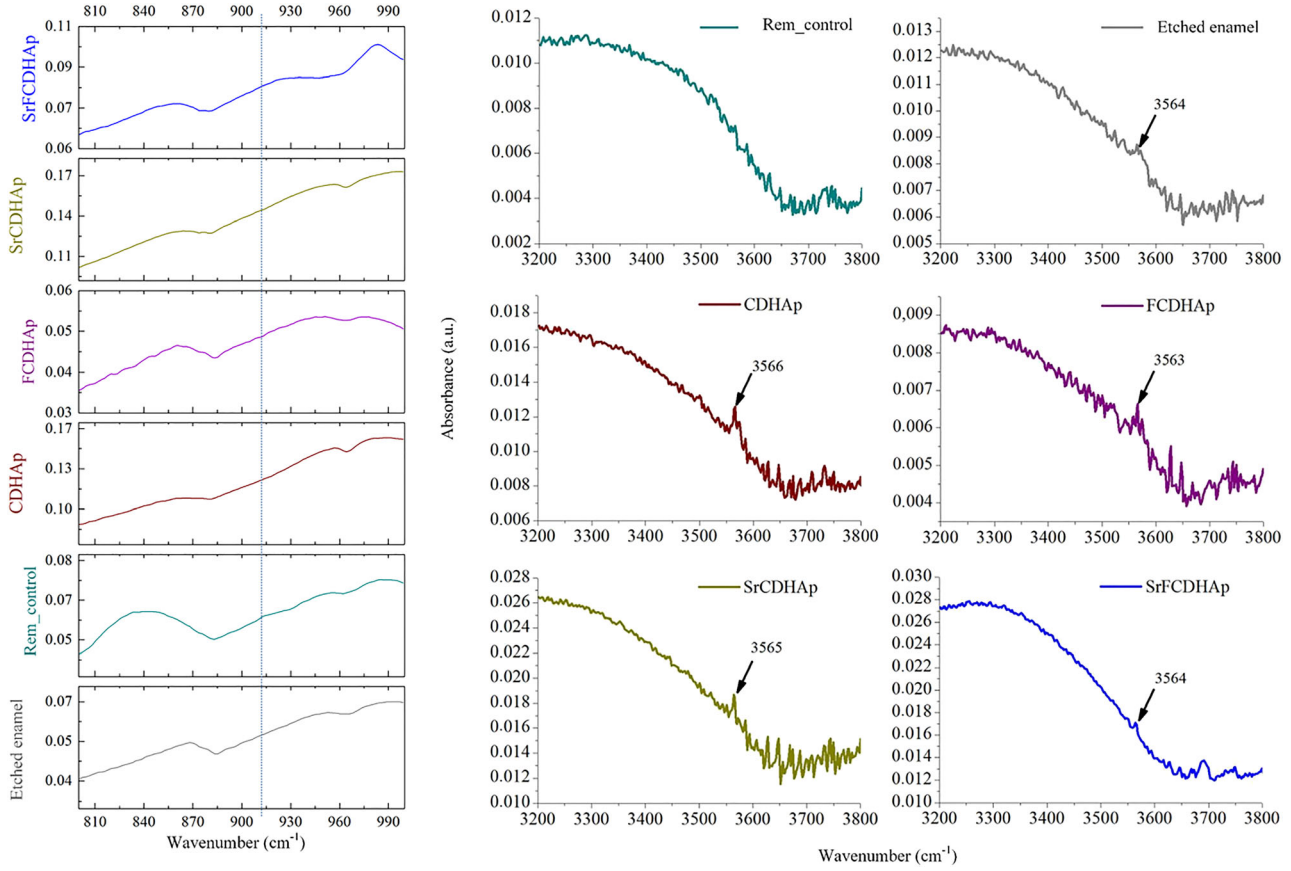

FIGURE 12 The zoomed in FTIR spectra: (A) OCP (800–990 cm^{-1}) and (B) (OH) (3200–3800 cm^{-1}) detection. FTIR, Fourier transformation infrared spectroscopy; OCP, octa-calcium phosphate

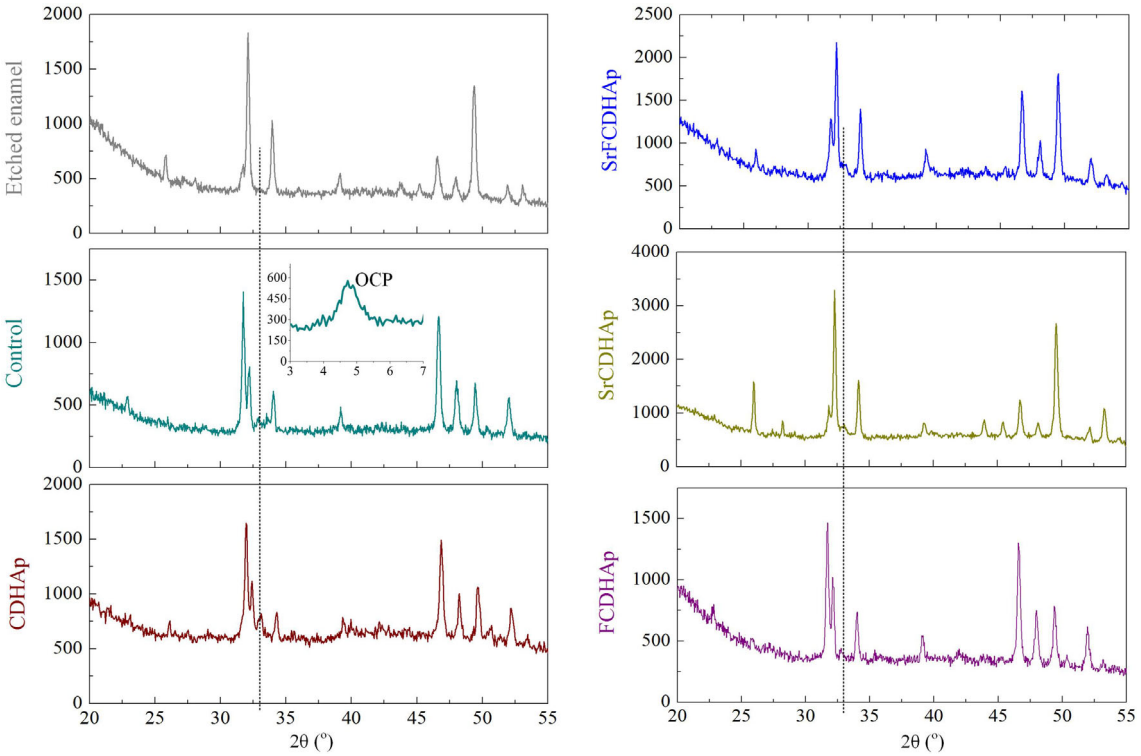

FIGURE 13 XRD patterns of the treated enamel samples. XRD, X-ray powder diffractometry

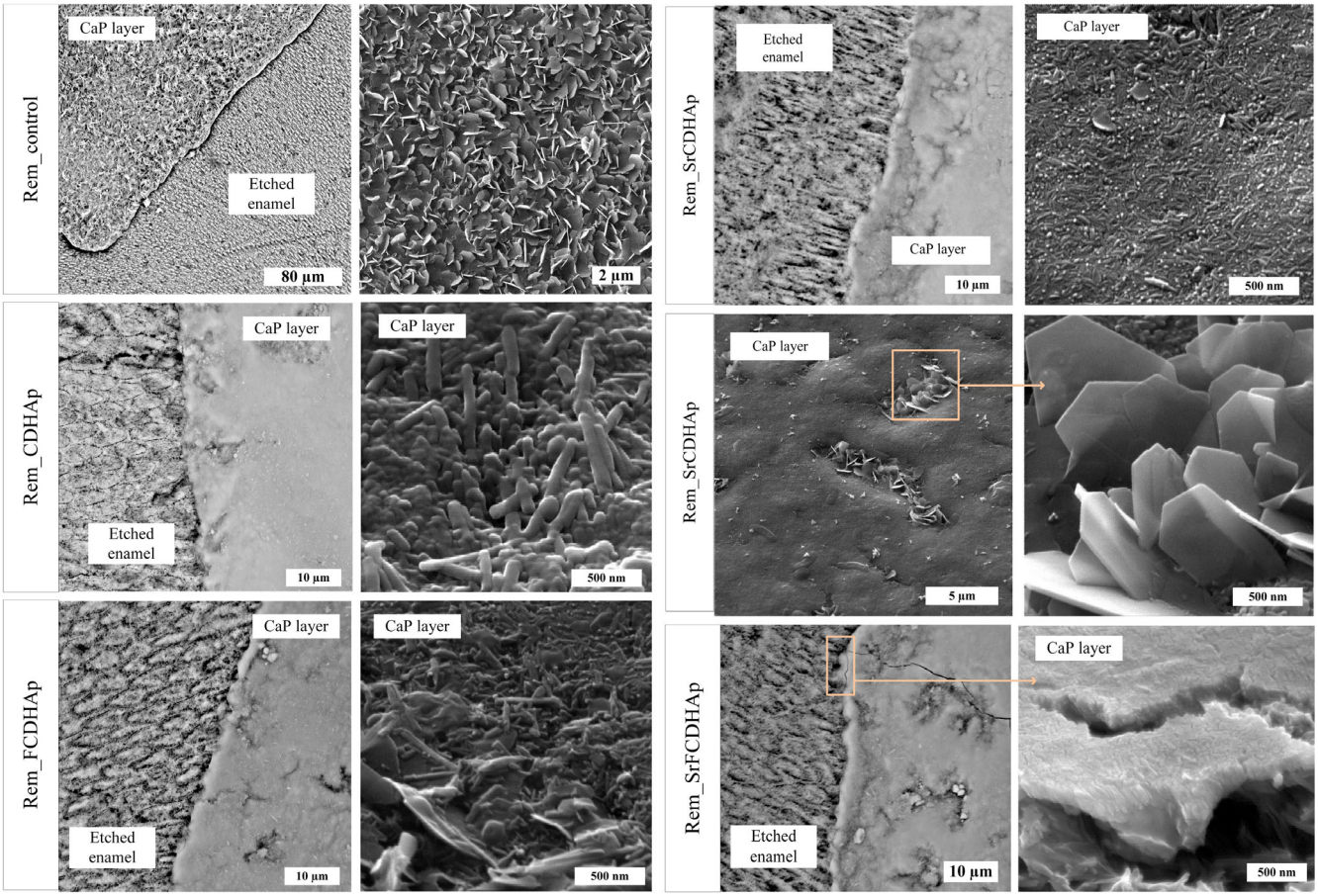

FIGURE 14 (A) SEM micrographs of Rem_control, (B) Rem_CDHAp, (C) Rem_FCDHAp, Rem_SrFCDHAp enamel samples. CDHAp, calcium deficient hydroxyapatite; FCDHAp, F substituted CDHAp; SEM, scanning electron microscopy

TABLE 4 EDX results for remineralized enamel samples

		F, wt %	Sr, wt %
Rem_Control	EE	–	–
	NL	–	–
Rem_CDHAp	EE	–	–
	NL	–	–
Rem_FCDHAp	EE	–	–
	NL	1.7 ± 0.8	–
Rem_SrCDHAp	EE	–	–
	NL	–	5.3 ± 0.6
Rem_SrFCDHAp	EE	–	–
	NL	1.3 ± 0.1	3.5 ± 0.2

Abbreviations: CDHAp, calcium deficient hydroxyapatite; EE-etched enamel; FCDHAp, F substituted CDHAp; NL-new CaP layer.

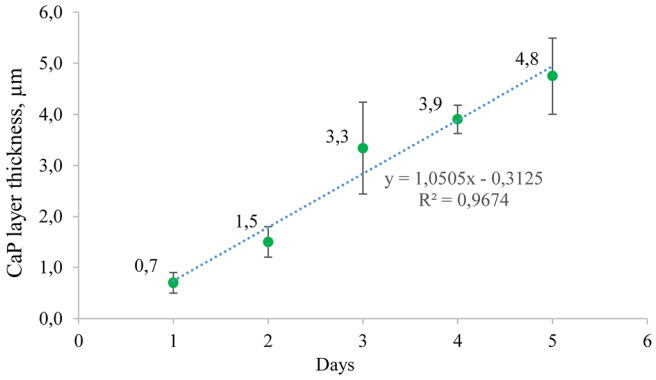

FIGURE 15 CaP layer formation kinetics (Rem_CDHAp sample group). CaP, calcium phosphates; CDHAp, calcium deficient hydroxyapatite

detected, but not for etched enamel. It should be noted that peaks have slight deviation compared to HAp record in the database. For Rem_CDHAp sample it was at 33.31° 2θ, for Rem_Control—32.89° 2θ, for Rem_SrFCDHAp—32.85° 2θ, for Rem_SrCDHAp—32.91° 2θ and for Rem_FCDHAp—32.93° 2θ. One additional peak was found for Rem_control at 4.8° 2θ, which is characteristic for OCP phase. (Figure 13)

3.4.3 | Scanning electron microscopy

SEM images (Figure 14) clearly showed morphological differences between treated and untreated enamel surfaces. A layer of plate-like crystals on the Rem_control surface was observed. According to XRD, FTIR results and literature,[47,48] the observed crystals are typical for OCP phase. Similar crystals were found in the hollows of

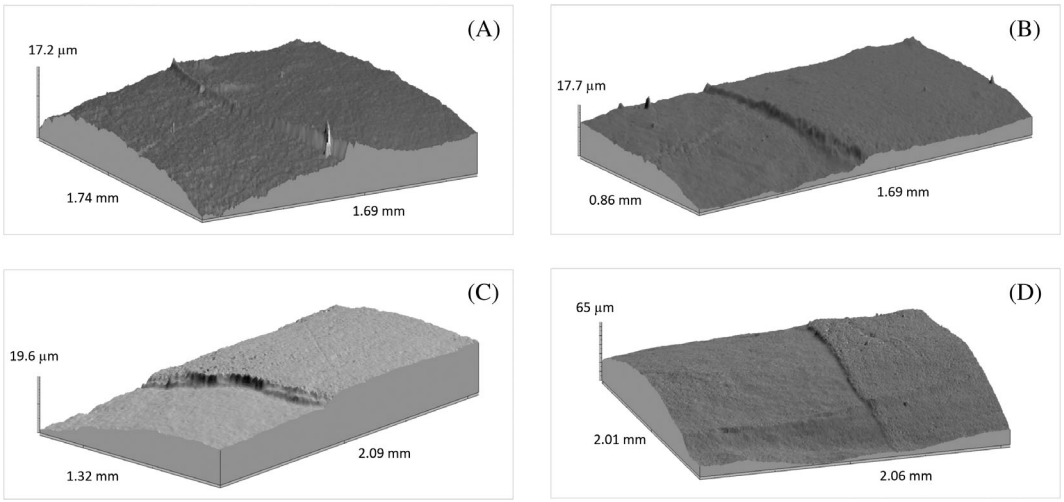

FIGURE 16 3D photo simulation of enamel surface (A—Rem_CDHAp, B—Rem_FCDHAp, C—Rem_SrCDHAp, D—Rem_SrFCDHAp). CDHAp, calcium deficient hydroxyapatite; FCDHAp, F substituted CDHAp

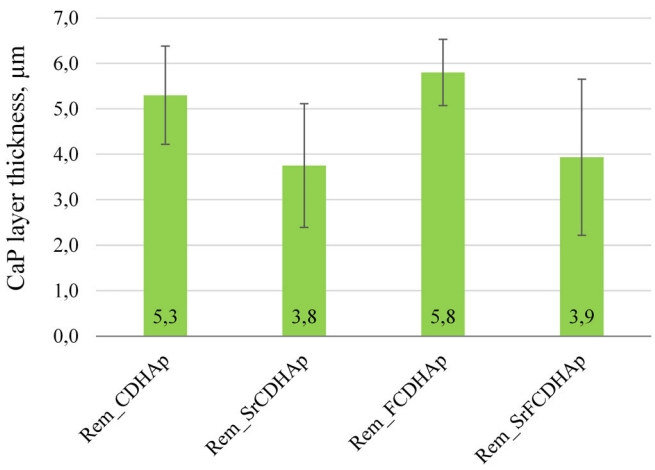

FIGURE 17 The thickness of new CaP layer on the enamel surface after 7 days in vitro treatment with CaP pastes (Comment: CaP layer was not detected on Rem_Control samples). CaP, calcium phosphates

Rem_SrCDHAp sample surface, although neither XRD nor FTIR detected OCP phase, because of proportionally small phase amount present on the sample.

New CaP layer formed on Rem_CDHAp, Rem_FCDHAp, Rem_SrCDHAp, and Rem_SrFCDHAp samples consisted of chaotically oriented rod-like CaP crystals. In the case of Rem_SrFCDHAp, there was evidence for crystal orientation (Figure 14E). Nonetheless, this observation has to be approved by further experiments.

3.4.4 | Energy-dispersive x-ray analysis

Along with SEM observation, EDX analysis was performed. The presence of F was detected for samples brushed with FCDHAp and SrFCDHAp paste, but Sr was found for samples brushed with SrCDHAp and SrFCDHAp paste (Table 4).

3.4.5 | Profilometry

The graph (Figure 15) demonstrated the kinetics of CaP layer formation in time. During the experiment, it was observed that the layer thickness increases linearly 0.8 ± 0.1 µm per day.

Figure 16 showed stepped border for each group. For Rem_control CaP layer was too thin to be detected by profilometry.

The results of profilometry (Figure 17) suggest the thickest CaP layer was for Rem_CDFHAp (5.3 ± 1.1 µm) and Rem_CDHAp (5.8 ± 0.7 µm), but seemingly thinner layer was observed for Rem_SrCDHAp (3.8 ± 1.4 µm) and Rem_SrFCDHAp (3.9 ± 1.7 µm). However, data analysis revealed that there is no statistical difference among groups.

4 | DISCUSSION

Precipitation methods for synthesis of CaP are popular due to their simplicity and possibility to perform chemical and morphological variations of the product. In our case the chosen technique justified, because F^- and Sr^{2+} ions were incorporated into CaP structure and morphology of particles was similar to HAp present in natural teeth enamel.[4] Moreover, obtained CaP products were calcium deficient and Ca/P ratio was comparable with natural teeth enamel, where Ca/P ratio is about 1.63.[2]

The highest SSA values were measured for SrCDHAp following by CDHAp, SrFCDHAp, and FCDHAp. We observed that fluoride incorporation into CDHAp structure results in lower values of SSA compared to CDHAp and SrCDHAp powders. In our study, it was 71.1 and 78.1 m^2/g. It is in agreement with L.M. Rodrıguez-Lorenzo

et al. research, where SSA below 100 g/m^2 was observed for HAp powders if fluoride content increases in its structure.[6]

It was interesting to test the ability of CaP particles to increase pH of acidic media, simulating environment in mouth after food consumption. Results (Figure 9) clearly demonstrated uplift for all CaP curves along the pH axis after incremental addition of acid, while for enamel piece the critical pH level was reached already after the first added volume of acid meaning irreversible dissolution of enamel minerals. Decrease of pH in the experimental system released phosphate ions in the solution, thus increased concentration of them. Other study has shown, that excess phosphate in the media increase solubility of HAp phase.[49] Interesting, that there are authors who suggest nano dissolution model for nanoparticles.[22,50,51] This model says that the active dissolution pits cannot be produced on nanoparticles, or more precisely, nano-sized particles could be kinetically stable in undersatured medium. This theory was proposed by S. Mafe et al. and confirmed by other researchers conducting in vitro experiments with natural enamel samples. In our case samples for pH test were powders, which mean that particles more easily can interact with surrounding media. If we combine observed pH increase effect with nano dissolution model for CaP particles it could be possible to get excellent protecting materials for tooth enamel. However, this judgment should be tested in studies. Additionally, SEM and TEM evaluation (Figure 8) confirmed needle-like morphology for all synthesized CaP. Nanoparticles morphology was close to natural tooth crystals 50–70 nm in width and 20–25 nm in thickness.[40] These observations suggested, if enamel surface would be covered with CaP layer, it could serve as protective coating and balance pH level at the enamel surface at the same time.

After in vitro study SEM images (Figure 14) and profilometry (Figure 16) clearly demonstrated border on the enamel samples surface where etched enamel and CaP layer can be distinguished. A larger SEM magnification revealed various textures of the CaP layers, but unifying feature was chaotically distributed rods-like particles in the sample surfaces. Only for Rem_SrFCDHAp sample crystal orientation was found. Interestingly, that plate-like OCP crystals covered surface of Rem_Control samples and also for Rem_SrCDHAp samples OCP crystals were locally distributed in the hollows. Formation of OCP crystals could be explained by the fact, that artificial saliva contained $H_2PO_4^-$ and Ca^{2+} ions and pH was adjusted to 7.4. These conditions favored formation of OCP phase on the enamel sample surface.[52] Another aspect is that OCP and HAp crystal structures are very similar and this reason often leads to epitaxial growth of these phases.[52] Additionally, J. Simmer et al. theorized that a unit-cell thickness of OCP hydrolyzes into a two-unit-cell thickness of OHAp and further hydrolysis lead to formation of HAp phase during enamel formation.[48]

Although, newly formed CaP layer was visible in SEM micrographs and profilometry results, XRD patterns and FTIR spectra of treated samples did not show the same results as for synthesized CaP powders that were expected. The explanation could be related to the depth of penetration of the respective beam into the sample, meaning that XRD and IR detectors received information not only from the CaP layer, but also from the natural enamel. As the enamel samples were taken from different teeth and different teeth surfaces, than the resulting XRD pattern intensities were various because HAp crystals in enamel are oriented differently.[53] Nevertheless, there was noticed one peak at 32.8 2θ for all remineralized samples that was not for etched enamel, which indicates that new layer was formed on samples surfaces. Additionally, a small peak from (OH) group vibration was detected (Figure 12B) in the FTIR spectra. Data from profilometry demonstrated linear increase of CaP layer thickness of 0.8 ± 0.1 μm per day, and the largest increase was detected for Rem_SrFCDHAp, but the lowest for Rem_SrCDHAp. However, data analysis revealed that there was no statistical difference among the groups. Thus, we can assume that nor fluoride, neither strontium in the CaP structure affected the thickness formation of new layer.

Thuy et al. in the study used a solution containing Sr^{2+}, F^-, Ca^{2+}, and H_2PO^{3-} ions to remineralize tooth enamel. After storing the samples in this solution for 14 days, the researchers found that the presence of Sr^{2+} and F^- contributed to the remineralization of the damaged enamel surface compared to the presence of fluoride alone in the remineralizing solution.[54] However, it should be noted that the form in which Sr and F come into contact with the enamel surface, that is, in the form of a free ion or bound in a structure, as it was in our research, could play an important role in such remineralization researches. Also, in order to make objective comparison of results and make study-based claims, the procedures for in vitro remineralization experiments should be standardized or very similar in different experiments.

All obtained results were supported by different instrumental methods and indicated CaP layer on the natural enamel surface. It is essentially that this layer formed even though the enamel blocks were faced downwards thus eliminating the deposition of CaP particles on the sample surface due to gravity.

In addition, it is known that a person loses minerals from the top layer of enamel from 10 to 40 μm due to erosion every year.[55] The addition of CaP nanoparticles (obtained in this study) in the oral care products, mainly toothpastes, could help not only to prevent the development of caries, but also to reduce enamel wear, because the CaP layer could initially dissolve, thus protecting natural enamel, but there should be further research carried out.

5 | CONCLUSION

Used modified wet precipitation technique was successfully applied for synthesis of CDHAp, SrCDHAp, FCDHAp, and SrFCDHAp nanoparticles. CDHAp and Sr and/or F substituted CDHAp nanoparticle suspensions had ability to increase pH level after addition of acid and maintain above pH 5.5, which is crucial for enamel dissolution. Developed CaP pastes provide formation of CaP layer on the etched bovine enamel samples in vitro. The thickness of layer increased by an average 0.8 μm per day reaching 5.6 μm after 7 days. There was no statistically reliable difference in in vitro results among Rem_CDHAp, Rem_SrCDHAp, Rem_FCDHAp, and Rem_SrFCDHAp. In conclusion,

from the results obtained we can expect that, if the enamel would be treated with one of the produced pastes containing synthesized CDHAp nanoparticles, the formation of CaP coating would occur and serve as sacrificial layer protecting the enamel from damages caused by acidic foods and caries.

For future, additional studies need to be performed to prove the formation of protective CaPs layer in in vivo conditions.

ACKNOWLEDGMENTS

This work has been supported by the European Regional Development Fund within the Activity 1.1.1.2 "Post-doctoral Research Aid" of the Specific Aid Objective 1.1.1 "To increase the research and innovative capacity of scientific institutions of Latvia and the ability to attract external financing, investing in human resources and infrastructure" of the Operational Programme "Growth and Employment" (No. 1.1.1.2/VIAA/3/19/459). The authors acknowledge financial support from the European Union's Horizon 2020 research and innovation programme under the grant agreement No 857287.

CONFLICT OF INTEREST

The authors report no declarations of interest.

DATA AVAILABILITY STATEMENT

The data that support the findings of this study are available from the corresponding author upon reasonable request.

ORCID

Vita Zalite https://orcid.org/0000-0002-4319-9334

REFERENCES

1. Dorozhkin SV. Biphasic, triphasic and multiphasic calcium orthophosphates. *Acta Biomater*. 2012;8:963-977.
2. Al-Sanabani JS, Madfa AA, Al-Sanabani FA. Application of calcium phosphate materials in dentistry. *Int J Biomater*. 2013;2013:1-12.
3. Boanini E, Gazzano M, Bigi A. Ionic substitutions in calcium phosphates synthesized at low temperature. *Acta Biomater*. 2010;6:1882-1894. http://www.ncbi.nlm.nih.gov/pubmed/20040384
4. Epple M, Baeuerlein E, eds. *Handbook of Biomineralization. Medical and Clinical Aspects*. WileVCH Verlag GmbH & Co; 2007.
5. Pan Y, Fleet ME. Compositions of the apatite-group minerals: substitution mechanisms and controlling factors. *Rev Miner Geochem*. 2002;48:13-49.
6. Rodríguez-Lorenzo L, Hart J, Gross K. Influence of fluorine in the synthesis of apatites. Synthesis of solid solutions of hydroxy-fluorapatite. *Biomaterials*. 2003 http://linkinghub.elsevier.com/retrieve/pii/S014296120300259X;24:3777-3785.
7. Zhuang Z, Yoshimura H, Aizawa M. Synthesis and ultrastructure of plate-like apatite single crystals as a model for tooth enamel. *Mater Sci Eng C*. 2013;33:2534-2540.
8. Stipniece L, Slama-Ancane K, Loca D, Pasatre S. Synthesis of strontium substituted hydroxyapatite through different precipitation routes. *Key Eng Mater*. 2016;674:3-8.
9. Lin K, Wu C, Chang J. Advances in synthesis of calcium phosphate crystals with controlled size and shape. *Acta Biomater*. 2014;10:4071-4102.
10. Taş A. Molten salt synthesis of calcium hydroxyapatite whiskers. *J Am Ceram Soc*. 2001;84:295-300.
11. Sadat-Shojai M, Khorasani MT, Dinpanah-Khoshdargi E, Jamshidi A. Synthesis methods for nanosized hydroxyapatite with diverse structures. *Acta Biomater*. 2013;9:7591-7621.
12. Lochaiwatana Y, Poolthong S, Hirata I, Okazaki M, Swasdison S, Vongsavan N. The synthesis and characterization of a novel potassium chloride-fluoridated hydroxyapatite varnish for treating dentin hypersensitivity. *Dent Mater J*. 2015;34:31-40. http://www.ncbi.nlm.nih.gov/pubmed/25748456
13. Gallo R. Synthesis and characterization of substituted apatites for biomedical applications. Universita Degli Studi di Padova. 2011; pp. 194.
14. Jalota S, Tas AC, Bhaduri SB. Microwave-assisted synthesis of calscium phosphate nanowhiskers. *J Mater Res*. 2004;19:1876-1880.
15. Jalota S, Bhaduri SB. ACT. In vitro testing of calcium phosphate (HA, TCP, and biphasic HA-TCP) whiskers. *J Biomed Mater Res Part A*. 2006;78:481-490. http://www.ncbi.nlm.nih.gov/pubmed/16948146
16. Cochrane NJ, Cai F, Huq NL, Burrow MF, Reynolds EC. New approaches to enhanced remineralization of tooth enamel. *J Dent Res*. 2010;89:1187-1197. http://www.ncbi.nlm.nih.gov/pubmed/20739698
17. Elkassas D, Arafa A. The innovative applications of therapeutic nanostructures in dentistry. *Nanomed Nanotechnol, Biol Med*. 2017;13:1543-1562.
18. Melo MAS, Guedes SFF, Xu HHK, Rodrigues LKA. Nanotechnology-based restorative materials for dental caries management. *Trends Biotechnol*. 2013;31:459. http://linkinghub.elsevier.com/retrieve/pii/S0167779913001194-467.
19. Iafisco M, Degli Esposti L, Ramírez-Rodríguez GB, et al. Fluoride-doped amorphous calcium phosphate nanoparticles as a promising biomimetic material for dental remineralization. *Sci Rep*. 2018;8:1-9.
20. Hannig M, Hannig C. Nanotechnology and its role in caries therapy. *Adv Dent Res*. 2012;24:53-57. http://www.ncbi.nlm.nih.gov/pubmed/22899680
21. El Gezawi M, Wölfle UC, Haridy R, Fliefel R, Kaisarly D. Remineralization, regeneration, and repair of natural tooth structure: influences on the future of restorative dentistry practice. *ACS Biomater Sci Eng*. 2019;5:4899-4919.
22. Li L, Pan H, Tao J, et al. Repair of enamel by using hydroxyapatite nanoparticles as the building blocks. *J Mater Chem*. 2008;18:4079.
23. Beltra-Aguilar ED, Goldstein JW, Lockwood SA. Fluoride varnishes. *J Am Dent Assoc*. 2000;131:589-596.
24. Mantzourani M, Sharma D. Dentine sensitivity: past, present and future. *J Dent*. 2013;41(Suppl 4):S3-S17. http://www.ncbi.nlm.nih.gov/pubmed/23929643
25. Domon-Tawaraya H, Nakajo K, Washio J, et al. Divalent cations enhance fluoride binding to streptococcus mutans and streptococcus sanguinis cells and subsequently inhibit bacterial acid production. *Caries Res*. 2013;47:141-149.
26. Pearce EI, Sissons CH. The concomitant deposition of strontium and fluoride in dental plaque. *J Dent Res*. 1987;66:1518-1522.
27. Enomoto A, Tanaka T, Kawagishi S, Nakashima H, Watanabe K, Maki K. Amounts of Sr and Ca eluted from deciduous enamel to artificial saliva related to dental caries. *Biol Trace Elem Res*. 2012;148:170-177.
28. Ten CJM, Featherstone JDB. Mechanistic aspects of the interactions between fluoride and dental enamel. *Crit Rev Oral Biol Med*. 1991;2:283-296.
29. Featherstone JDB. The science and practice of caries prevention. *J Am Dent Assoc*. 2000;131:887-899.
30. Dabsie F, Gregoire G, Sixou M, Sharrock P. Does strontium play a role in the cariostatic activity of glass ionomer? Strontium diffusion and antibacterial activity. *J Dent*. 2009 http://www.ncbi.nlm.nih.gov/pubmed/19410352;37:554-559.
31. Krishnan V, Bhatia A, Varma H. Development, characterization and comparison of two strontium doped nano hydroxyapatite molecules for enamel repair/regeneration. *Dent Mater*. 2016;32:646-659.

32. Bracci B, Torricelli P, Panzavolta S, Boanini E, Giardino R, Bigi A. Effect of Mg(2+), Sr(2+), and Mn(2+) on the chemico-physical and in vitro biological properties of calcium phosphate biomimetic coatings. *J Inorg Biochem*. 2009;103:1666-1674. http://www.ncbi.nlm.nih.gov/pubmed/19819556
33. Al-Khafaji TJ, Wong F, Fleming PS, Karpukhina N, Hill R. Novel fluoride and strontium-containing bioactive glasses for dental varnishes-design and bioactivity in tris buffer solution. *J Non Cryst Solids*. 2019;503-504:120-130.
34. Dai LL, Mei ML, Chu CH, Lo ECM. Remineralizing effect of a new strontium-doped bioactive glass and fluoride on demineralized enamel and dentine. *J Dent*. 2021;108:103633.
35. Dai LL, Nudelman F, Chu CH, Lo ECM, Mei ML. The effects of strontium-doped bioactive glass and fluoride on hydroxyapatite crystallization. *J Dent*. 2021;105:103581.
36. Simila HO, Karpukhina N, Hill RG. Bioactivity and fluoride release of strontium and fluoride modified biodentine. *Dent Mater*. 2018;34:e1-e7.
37. Karampas IA, Kontoyannis CG. Characterization of calcium phosphates mixtures. *Vib Spectrosc*. 2013;64:126-133.
38. Chung H-Y, Li C-C, Hsu C-C. Characterization of the effects of 3DSS peptide on remineralized enamel in artificial saliva. *J Mech Behav Biomed Mater*. 2012 http://www.ncbi.nlm.nih.gov/pubmed/22301175;6:74-79.
39. Liga Berzina-Cimdina NB. Research of calcium phosphates using Fourier transform infrared spectroscopy. In: Theophanides T, ed. *Infrared Spectroscopy Materials Science Engineering and Technology*. InTech; 2012.
40. Moradian-Oldak J. Protein-mediated enamel mineralization. *Front Biosci*. 2012;17:1996-2023.
41. Dorozhkin SV. Calcium orthophosphates in dentistry. *J Mater Sci Mater Med*. 2013;24:1335-1363.
42. Zulkifli FH, Hussain FSJ, Zeyohannes SS, Rasad MSBA, Yusuff MM. A facile synthesis method of hydroxyethyl cellulose-silver nanoparticle scaffolds for skin tissue engineering applications. *Mater Sci Eng C*. 2017;79:151-160.
43. Diao Y, Song M, Zhang Y, Shi L, Ying LY, Ran R. Enzymic degradation of hydroxyethyl cellulose and analysis of the substitution pattern along the polysaccharide chain. *Carbohydr Polym*. 2017;169:92-100.
44. Orhan B, Ziba CA, Morcali MH, Dolaz M. Synthesis of hydroxyethyl cellulose from industrial waste using microwave irradiation. *Sustain Environ Res*. 2018;28:403-411.
45. Sa Y, Liang S, Ma X, et al. Compositional, structural and mechanical comparisons of normal enamel and hypomaturation enamel. *Acta Biomater*. 2014;10:5169-5177. http://www.sciencedirect.com/science/article/pii/S1742706114003596
46. Zhuang Z, Yamamoto H, Aizawa M. Synthesis of plate-shaped hydroxyapatite via an enzyme reaction of urea with urease and its characterization. *Powder Technol*. 2012;222:193-200.
47. Wang L, Guan X, Du C, Moradian-Oldak J, Nancollas GH. Amelogenin promotes the formation of elongated apatite microstructures in a controlled crystallization system. *J Phys Chem C Nanomater Interfaces*. 2007;111:6398-6404.
48. Simmer JP, Fincham AG. Molecular mechanisms of dental enamel formation. *Crit Rev Oral Biol Med*. 1995;6:84-108.
49. Liu Q, Chen Z, Pan H, Darvell BW. The effect of excess phosphate on the solubility of hydroxyapatite. *Ceram Int*. 2014;40:2751-2761.
50. Mafé S, Manzanares JA, Reiss H, Thomann JM, Gramain P. Model for the dissolution of calcium hydroxyapatite powder. *J Phys Chem*. 1992;96:861-866.
51. Wang L, Tang R, Bonstein T, Orme CA, Bush PJ, Nancollas GH. A new model for nanoscale enamel dissolution. *J Phys Chem B*. 2005;109:999-1005.
52. Wang L, Nancollas GH. Calcium orthophosphates: crystallization and dissolution. *Chem Rev*. 2008;108:4628-4669.
53. Fujisaki K, Todoh M, Niida A, Shibuya R, Kitami S, Tadano S. Orientation and deformation of mineral crystals in tooth surfaces. *J Mech Behav Biomed Mater*. 2012;10:176-182.
54. Thuy TT, Nakagaki H, Kato K, et al. Effect of strontium in combination with fluoride on enamel remineralization in vitro. *Arch Oral Biol*. 2008 http://www.ncbi.nlm.nih.gov/pubmed/18672228;53:1017-1022.
55. Zheng J, Li Y, Shi MY, Zhang YF, Qian LM, Zhou ZR. Microtribological behaviour of human tooth enamel and artificial hydroxyapatite. *Tribol Int*. 2013 http://linkinghub.elsevier.com/retrieve/pii/S0301679X12001430;63:177-185.

How to cite this article: Zalite V, Lungevics J, Vecstaudza J, Stipniece L, Locs J. Nanosized calcium deficient hydroxyapatites for tooth enamel protection. *J Biomed Mater Res*. 2021;1-14. doi:10.1002/jbm.b.35005